

Friction Hydro-Pillar Processing of a High Carbon Steel: Joint Structure and Properties



LUIS FERNANDO KANAN, BUCHIBABU VICHARAPU, ANTONIO FERNANDO BURKERT BUENO, THOMAS CLARKE, and AMITAVA DE

A coupled experimental and theoretical study is reported here on friction hydro-pillar processing of AISI 4140 steel, which is a novel solid-state joining technique to repair and fill crack holes in thick-walled components by an external stud. The stud is rotated and forced to fill a crack hole by plastic flow. During the process, frictional heating occurs along the interface of the stud and the wall of crack hole leading to thermal softening of the stud that eases its plastic deformation. The effect of the stud force, its rotational speed and the total processing time on the rate of heat generation and resulting transient temperature field is therefore examined to correlate the processing variables with the joint structure and properties in a systematic and quantitative manner, which is currently scarce in the published literature. The results show that a gentler stud force rate and greater processing time can promote proper filling of the crack hole and facilitate a defect-free joint between the stud and original component.

<https://doi.org/10.1007/s11663-018-1171-5>

© The Minerals, Metals & Materials Society and ASM International 2018

I. INTRODUCTION

FRICITION hydro-pillar processing (FHPP) is a new solid-state joining technology with unique application such as filling of surface and sub-surface cracks in thick-walled vessels of steels.^[1] For example, FHPP was recently attempted for the first time to repair cracks in space shuttle external components of high-strength aluminum alloys.^[2] FHPP is also considered in repairing surface cracks in steam turbine rotors of a high-strength, high-temperature-resistant steel (grade 26NiCr-MoV14-5).^[3] Alternative methods such as fusion welding processes for in-service repairing of cracks in components of these high-strength steels remained difficult because of their high hardenability and mandatory need of pre-heating and post-weld heat treatment (PWHT).^[4,5] In contrast, initial FHPP trials could achieve joint strengths up to 90 pct of the base materials in high-strength steel components, especially those used for petrochemical and thermal power plants.^[6-9] In particular, pressurized pipes and vessels of AISI 4140 steel are widely used in the power generation, oil and gas, and petrochemical industries. Initial studies on

FHPP of this alloy have showed promising results. The present work is therefore aimed at probing a systematic investigation of FHPP of AISI 4140 steel.

Fusion welding of AISI 4140 steel is usually recommended in annealed condition and with low hydrogen diffusible filler wires of relatively lower strength, *e.g.*, ER70S-2 and ER80S-D2, because of the very high hardenability of AISI 4140 steel.^[10] Careful pre-heating and PWHT procedures must be followed to avoid cold cracking, reduce residual stresses and decrease impairment of HAZ properties in fusion welding of AISI 4140 steel.^[11] Since FHPP is a solid-state joining process, several of the aforementioned issues can be alleviated. A systematic analysis of FHPP of AISI 4140 is therefore needed but scarce in the literature.

The effect of stud force and stud rotational speed on joint structure and properties was studied briefly in FHPP of AISI 4140 steel.^[7] A combination of high stud rotational speed of 6000 rpm and a low stud force of 10.5 kN provided fair joint properties that were comparable to those of the base materials.^[7] An increase in stud force led to faster plastic flow of the stud and therefore reduced the overall processing time and peak temperature.^[1,12] However, the effect of the reduced processing time and lower peak temperature on the joint properties were not well addressed in the literature. Improper selection of the stud force often led to “*lack of filling*” defects near the crack hole bottom in FHPP of high-strength steels.^[13] FHPP is also attempted under the water to reduce the peak temperature in components of high-strength line pipe X65 steels.^[8] However, the resulting joint exhibited a full martensite structure due to higher cooling rates.^[8] A fairly uniform hardness

LUIS FERNANDO KANAN, ANTONIO FERNANDO BURKERT BUENO, and THOMAS CLARKE are with the Universidade Federal do Rio Grande do Sul (UFRGS), Porto Alegre, RS 90035-190, Brazil. Contact e-mail: tclarke@demet.ufrgs.br BUCHIBABU VICHARAPU and AMITAVA DE are with the Indian Institute of Technology Bombay, Mumbai, Maharashtra, 400076, India.

Manuscript submitted October 3, 2017.

Article published online January 29, 2018.

distribution across the joint was reported in FHPP of C-Mn steel especially at lower stud forces.^[14] Although these studies provided an insight into FHPP of steels, a quantitative understanding of the effect of process variables on the temperature field, cooling rate and resulting joint hardness distribution remained scarce in FHPP of high-strength steels.

In FHPP, the real-time monitoring of temperature is challenging because of the continuous plastic deformation of the stud material inside the crack hole.^[15] Therefore, numerical modeling of FHPP was considered as a recourse to compute the evolution of the temperature field, thermal cycles and cooling rate in FHPP. Vicharapu *et al.*^[14] showed that the evolution of temperature field, thermal cycles and cooling rate in the joint area could be realized using a numerical heat transfer model in a preliminary study on FHPP of ASTM A36 steels. A coupled experimental and numerical investigation is therefore undertaken on FHPP of AISI 4140 steel. The effect of force rate on the rate of heat generation, thermal softening and plastic deformation of the stud, and the overall processing time was studied in a comprehensive manner. A two-dimensional axi-symmetric transient heat transfer analysis was carried out to compute the temperature distribution and thermal cycles. The computed thermal cycles were tested with the corresponding measured results and used to estimate the hardness distribution in the joint area following available empirical relations. The estimated hardness distributions were also tested with the corresponding measured results.

II. EXPERIMENTAL SET-UP AND PROCEDURE

Figure 1(a) shows the experimental set-up for FHPP in a schematic manner. The legends F , N and L refer to the stud force and its rotational speed and the length of the stud pushed into the crack hole, respectively. Figure 1(b) shows the typical nature of variations of the stud rotational speed and force and its insertion into the crack hole in three consecutive periods that are referred to as the dwell (t_1), burn-off (t_2) and forging (t_3) stages. All the FHPP experiments were conducted using a specially designed force-controlled displacement of the stud at the LAMEF-UFRGS, Brazil.^[12] Table I presents the chemical composition of the stud and substrate materials, both of which are taken as AISI 4140 steel.

As indicated in Figure 1(b), the stud force rises at a pre-set rate during the dwell stage to a constant value. As a result, heating due to friction occurs along the interface of the stud and base of the crack hole leading to thermal softening and plastic flow of the stud. Part of the plasticized stud is also allowed to come out as a flash to ensure adequate filling of the crack hole, which marks an end of the burn-off period, and the stud rotation is stopped. A constant stud force is still maintained, and often the same is augmented, to facilitate the consolidation of the plasticized material inside the crack hole and form a solid-state joint with the original component in the forging stage. Previous studies showed the

presence of typical voids at the root of the crack hole in FHPP of DH36 steel^[16] and AISI 4140 steel.^[7] In underwater FHPP of SS235 stainless steel, voids were found near the crack-hole base, which was attributed to inadequate heat generation and insufficient plastic flow of the stud material at the initial period.^[17] In underwater FHPP of X65 line pipe steels, the “*lack of filling*” defect near the crack-hole base was observed, which was attributed to insufficient stud force.^[8] Therefore, the force rate in dwell stage was considered as one of the main process variables in the present study for the first time in the FHPP literature.

Three different stud force rates were considered in the dwell stage as shown in Table II. The maximum stud length to be forced into the crack hole, referred to as the burn-off length, the stud rotational speed during the dwell and burn-off stages, and the final stud force in the burn-off and forging periods were kept constant at 7 mm, 5000 rpm and 25 kN, respectively (Table II). The dwell time (t_1) ends as the final stud force of 25 kN or the maximum burn-off length of 7.0 mm is reached at a given stud force rate. At higher force rates of 4.0 and 8.0 kN/s, the maximum stud burn-off length of 7.0 mm was consumed while a burn-off length of 6.5 mm could be used at the lower force rate of 2.0 kN/s (Table II). The burn-off time (t_2) allows further pushing of the stud into the crack hole to ensure adequate filling of the crack hole. However, the burn-off time (t_2) is eliminated if the crack hole is already filled with flashes emerging out by the end of the dwell stage (t_1). In contrast to dwell (t_1) and burn-off (t_2) times, the forging time (t_3) is a pre-set process variable.^[14]

Figures 2(a) and (b) show the stud and crack-hole geometries used for the experiments. Three K-type thermocouples of 1.0 mm diameter were located just outside the crack-hole wall at three different heights from the crack-hole base as shown in Figure 2(c). Each thermocouple was calibrated according to ASTM E230/E230M^[18] and spot-welded in a pre-drilled hole. The thermal cycles were measured at a simultaneous sampling rate of 5.0 Hz. Transverse joint sections were polished and etched with Nital solution to view the joint macrographs. Figure 2(c) also shows the locations used to measure Vicker’s micro-hardness, which was evaluated using a load of 0.5 kg and holding time of 10 seconds.

III. THEORETICAL FORMULATION

A transient heat transfer analysis was conducted considering the governing equation in the two-dimensional cylindrical coordinate system as

$$\frac{1}{r} \frac{\partial}{\partial r} \left(kr \frac{\partial T}{\partial r} \right) + \frac{\partial}{\partial z} \left(k \frac{\partial T}{\partial z} \right) + \dot{Q} = \rho C_p \frac{\partial T}{\partial t} \quad [1]$$

where k , ρ , C_p , T and t referred to the thermal conductivity, density, specific heat, and temperature and time variables, respectively. The term \dot{Q} accounts for the rate of heat generation along the interface of the stud and wall of the crack hole as

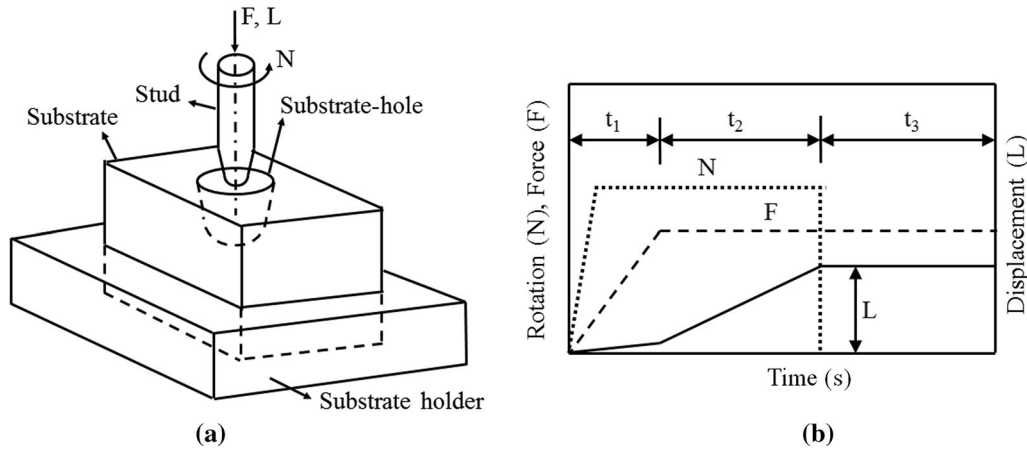


Fig. 1—(a) Schematic diagram of the FHPP setup and (b) typical responses of stud rotational speed (N), stud force (F) and stud burn-off length (L) in dwell (t_1), burn-off (t_2) and forging (t_3) stages, where t_1 , t_2 and t_3 indicate respective time durations.

Table I. Chemical Composition (in Wt Pct) of AISI 4140 Steel

C	Cr	Mo	Si	P	S	Mn	Ni
0.4	0.9	0.2	0.2	0.01	0.01	0.85	< 0.005

Table II. Process Conditions Considered in FHPP of AISI 4140 Steel

Rotational Speed (N , rpm)	Burn-off Length (L , mm)	Force (F , kN)		Force Rate in Dwell Stage (kN/s)	Processing Times (s)		
		Burn-off Stage	Forging Stage		Dwell Stage (t_1)	Burn-off Stage (t_2)	Forging Stage (t_3)
5000	6.5	25	25	2.0	12.5	0.0	15
	7.0			4.0	6.2	6.5	
	7.0			8.0	3.2	10.5	

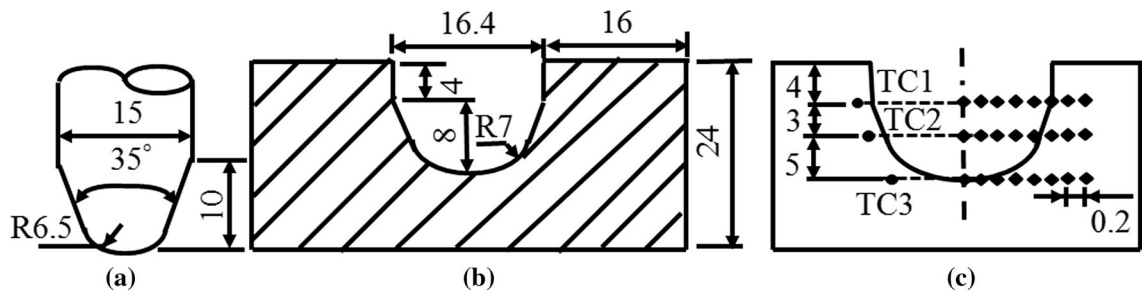


Fig. 2— Schematic diagrams of (a) stud, (b) substrate with crack hole, and (c) thermocouple and micro-hardness measurement locations. All dimensions are in mm.

$$\dot{Q} = [\eta_m(1 - \delta)\tau_y + \delta\mu_f P](r_1\omega)(A_i/V_i) \quad [2]$$

where η_m is the fractional mechanical work converted to heat, P the axial pressure on the stud, ω the stud angular speed, r_1 the radial distance of any point from the stud axis and τ_y the temperature dependent shear yield strength of stud material at r_1 . The value of η_m was considered as 0.3 based on a similar range of values used in modeling of friction stir welding.^[19,20] The

terms A_i and V_i refer to the contact area and volume of an element associated with the interface. The terms δ and μ_f refer to the local variations in fractional sliding and co-efficient of friction along the joint interface and are considered as

$$\delta = -0.026 + 0.275\exp(r_1\omega/1.87); \mu_f = 0.5\exp(-\delta r_1\omega) \quad [3, 4]$$

following similar expressions used in modeling of friction stir welding^[19] and FHPP of A36 steel.^[14] A

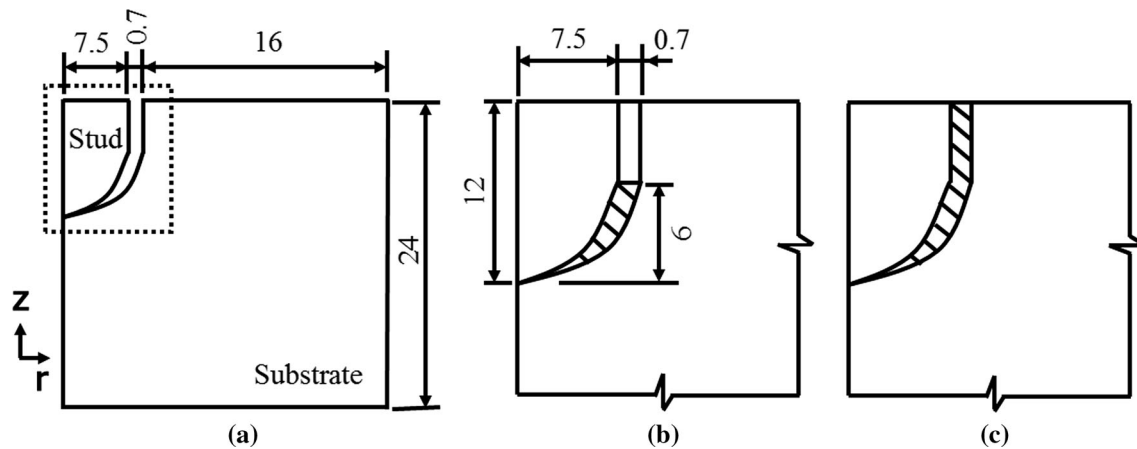


Fig. 3—(a) Schematic diagram of the solution domain considered for the numerical model. Computed results are shown for the dotted portion in zoomed view. Schematic diagrams (b) and (c) respectively show partially filled and fully filled stud-crack-hole clearances.

Table III. Thermo-physical Properties of AISI 4140 Steel^[22]

Density (kg/m ³)	7830
Solidus Temperature (K)	1750
Thermal conductivity (W/mK)	54.91–3.33e ⁻² × T + 1.0e ⁻⁵ × T ² for T < 1200 K 30.0 for T ≥ 1200 K
Specific Heat (J/kgK)	361.55 + 1.13e ⁻¹ + 3.0e ⁻⁴ × T ² 300 K ≤ T ≤ 1200 K 607.0 for T > 1200 K
Yield Strength (MPa)	919.61–1.21 × T + 4.21e ⁻⁴ × T ² for T ≤ 1200 K 13.0 for T > 1200 K

lumped heat transfer coefficient (h) was used to account for the convective heat loss from the surfaces as

$$h = h_b \times (T - T_0)^{0.25} \quad [5]$$

where $h_b = 65 \text{ W/m}^2 \text{ K}^{1.25}$.

Figure 3(a) shows the solution domain including the stud, crack hole and substrate considered for the heat transfer analysis. Figures 3(b) and (c) show schematic presentations of the solution domain with the stud-crack-hole clearance filled partially and completely. The filling of the stud-crack-hole clearance by the plasticized material was considered uniformly in an incremental manner through a number of discrete time steps.^[14] The hardness distribution across the joint area was estimated as a function of the cooling rate and hold time between the temperature range of 1073 K to 773 K (800 °C to 500 °C) following available analytical relations for alloys of similar compositions.^[21] The empirical relations used for hardness calculations are presented in Appendix A. The cooling rate and hold time between the specified temperature ranges were obtained from the numerically computed results. The model calculations considered temperature-dependent material properties (Table III).

IV. RESULTS AND DISCUSSION

Figure 4 shows the FHPP joint macrographs at three different force rates with the dashed lines highlighting

the original crack-hole boundary. The black slots, three in each case, with taper ends were used to fix the thermocouples for measurement of thermal cycles. In each case, the crack hole is completely filled by plastically deformed stud material as noted in Figure 4(a) through (c). At a force rate of 2.0 kN/s, the joint was free of any void or “lack of filling” as indicated in Figure 4(a). In contrast, a small crack-like defect is noted near the bottom of the crack hole for the FHPP joint made at the force rate of 4.0 kN/s as shown in Figure 4(b). The zoomed view of the defect region is shown in Figure 4(d) although the same does not exhibit a large void or network of small cracks.

Figure 4(c) shows the FHPP joint at the highest force rate of 8.0 kN/s with several small discontinuities near the base of the crack hole as indicated by two red color boxes. The zoomed views of these two defect regions are shown in Figures 4(e) and (f), which exhibits the network of discontinuities in the processed zone. Rise in force rate promotes a faster insertion of the stud inside the crack hole at a shorter dwell period resulting in inadequate thermal softening and localized discontinuities. Similar defects were reported by Meyer^[13] and Cui *et al.*^[17] in FHPP of X65 and S355 steels, respectively. Overall, the joints prepared at the force rate of 2.0 kN/s exhibited defect-free joints.

Figures 5(a) through (c) show the computed temperature isotherms at three different force rates of 2.0 kN/s, 4.0 kN/s and 8.0 kN/s, respectively, at a time instant of 3.2 seconds, which confirms to the end of the dwell stage at the force rate of 8.0 kN/s (Table II). The two white

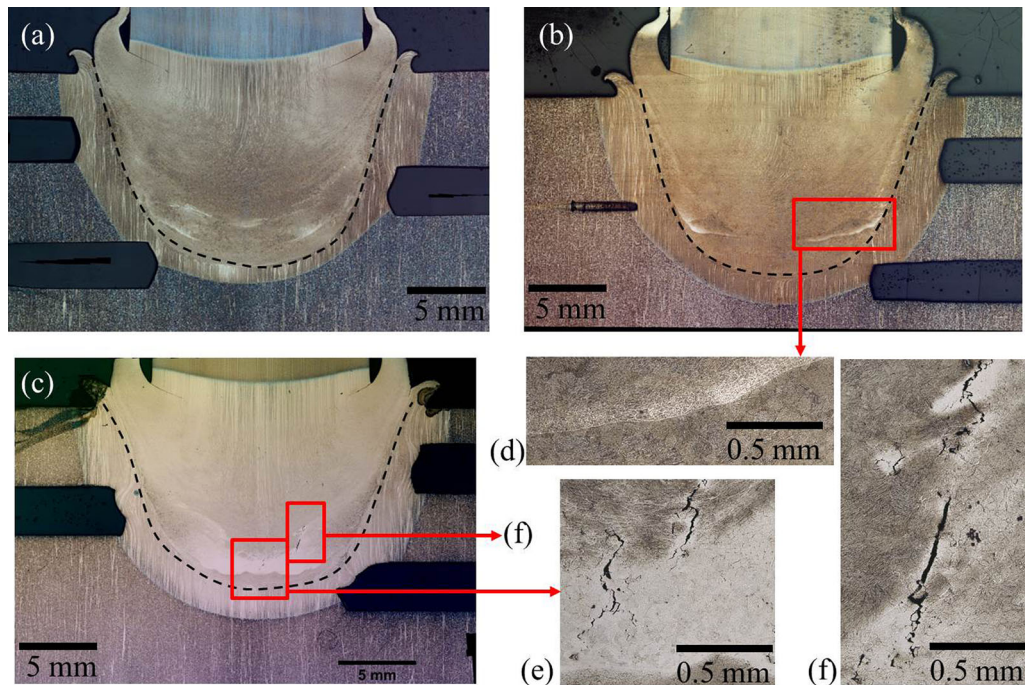


Fig. 4— Macrographs of the joints at different force rates (kN/s) of (a) 2.0, (b) 4.0 and (c) 8.0. Regions highlighted in red color in macrographs (b) and (c) show defects in the processed zone. Image (d) is a magnified view of the highlighted area in (b) showing no indication of lack of filling or cracks. Images (e) and (f) are the magnified views of defects in (c) (Color figure online).

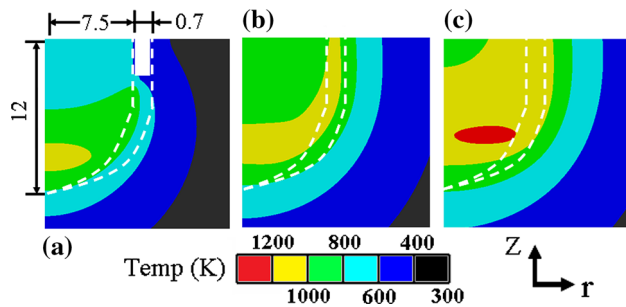


Fig. 5— Computed isotherms at time instant of 3.2 s at stud force rate (kN/s) of (a) 2.0, (b) 4.0 and (c) 8.0 during FHPP of AISI 4140 steel (Color figure online).

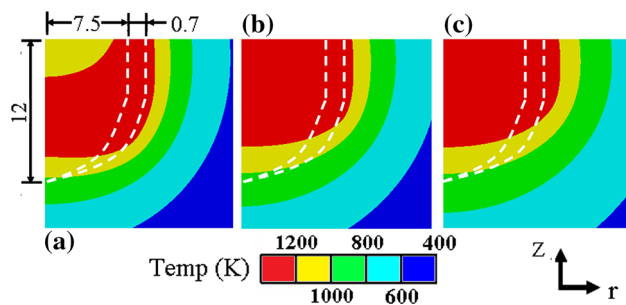


Fig. 6— Computed isotherms at time instant of 12.5 s at stud force rates (kN/s) of (a) 2.0, (b) 4.0 and (c) 8.0 during FHPP of AISI 4140 steel (Color figure online).

dashed lines in Figure 5 depict the original stud boundary and the wall of the crack hole; thus, the region enclosed between these two lines depicts the original

clearance to be filled up by deformed stud material. Figure 5(a) shows that at the force rate of 2.0 kN/s, the clearance between the stud and the crack hole is not yet filled up at the end of 3.2 seconds. In contrast, the crack hole is completely filled up at the other two force rates of 4.0 and 8.0 kN/s as depicted in Figures 5(b) and (c). A comparison of Figures 5(a) through (c) show that the maximum temperature towards the base of the crack hole tends to reduce with an increase in force rate at the time instant of 3.2 seconds. This was attributed to the rapid introduction and deformation of the stud at higher force rates that allowed less time for frictional heating. In contrast, a lower force rate allowed adequate time to frictional heating and ease of plastic deformation of the stud material along the interface of stud and base of the crack hole.

Figures 6(a) through (c) show the computed temperature isotherms at the time instant of 12.5 seconds, which corresponds to the end of the dwell stage at the lowest force rate of 2.0 kN/s. Figure 6(a) shows that the crack hole is filled up even at the lowest force rate of 2.0 kN/s. Further, almost the complete stud exhibited the maximum temperature of 1200 K for all the force rates. At the lowest force rate of 2.0 kN/s, the stud force reached to the maximum value of 25 kN at the end of 12.5 seconds, while at higher force rates of 4.0 and 8.0 kN/s, the maximum force was attained earlier as 6.5 and 3.2 seconds, respectively (Table II). As a result, the hotter region of the stud widened with a rise in force rates.

Quantitative knowledge of the thermal cycles and cooling rate is considered requisite to assess the structure and properties of the joint region in FHPP.

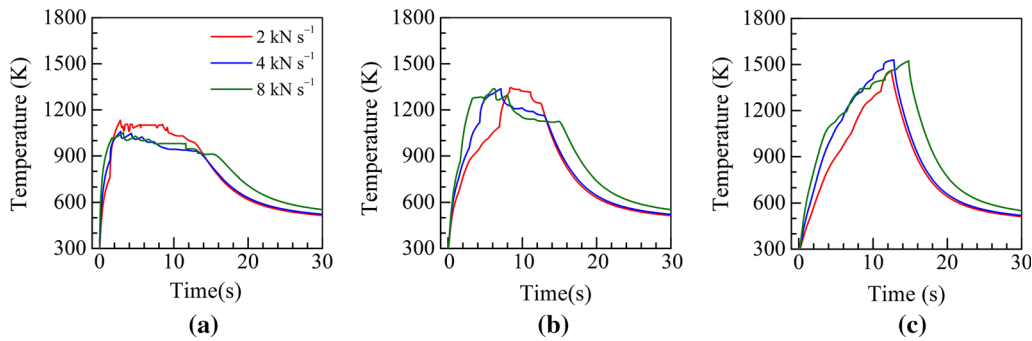


Fig. 7— Computed thermal cycles at different stud radii (mm) and heights (mm) from the crack-hole base as (a) (2.0, 0.0), (b) (3.0, 3.0) and (c) (3.7, 6.0) (Color figure online).

Figures 7(a) through (c) show the computed thermal cycles at three different locations, which are considered within the stud and at three different heights from the crack-hole base. Figure 7(a) shows the thermal cycles at the location very close to the crack-hole base. The thermal cycles in Figure 7(a) depict a rapid rise to a peak followed by a gentle cooling up to a certain time and then faster cooling. The initial rise in temperature is due to the heat generation caused by friction along the interface of the stud and crack-hole base. As the plasticized stud material deforms and piles up through the stud-crack-hole clearance, heat dissipation through the bulk material increases, leading to gradual cooling of the joint region near the crack-hole base. At the end of the dwell and burn-off stages, the stud rotation stops, leading to no further heat generation, and the interface cools down faster. Figure 7(a) implies a slightly higher peak temperature at the lowest force rate of 2 kN/s, which is attributed to the slower rate of introduction of the stud and consequent delayed filling of the stud-crack-hole clearance volume by plasticized stud material.

Figure 7(b) shows the computed thermal cycles at a height of 3 mm from the crack-hole base for all three force rates. The peak temperature in each case is higher and also attained at later time instants compared with that in Figure 7(a) as the filling of stud-crack-hole clearance occurs gradually from the bottom. Figure 7(b) also shows the peak temperatures reached after a certain time instant that nearly corresponds to the time to fill the height of 3 mm along the stud-crack-hole clearance zone at different force rates. The faster cooling in Figure 7(b) corresponds to the end of the dwell and burn-off stages when the stud rotation and thus frictional heat generation stops. The computed thermal cycles in Figure 7(c) are at a height of 6 mm from the crack-hole base and attained further delayed and higher peak temperature. Thus, the computed thermal cycles in Figures 7(a) through (c) could embody the effects of frictional heat generation, filling of stud-crack-hole clearance by plasticized material, heat dissipation through the bulk material and subsequent cooling as they occurred in different locations of the joint region during FHPP.

Figures 8(a) through (c) show the computed and corresponding measured thermal cycles at two different

thermocouple monitoring locations, TC1 and TC2 (Figure 2(c)). The measured peak temperatures increased steadily with a rise in stud force rates, as was expected. As a result, the measured cooling rates at TC1 increased from 41.66 to 57.69 K/s and at TC2 from 35.36 to 46.15 K/s with a rise in force rates from 2.0 to 8.0 kN/s. The computed peak temperatures and cooling rates were within 4.6 pct error with the corresponding measured results at the lowest stud force rate of 2.0 kN/s (Figure 8(a)). At the highest force rate of 8.0 kN/s, the computed peak temperatures and cooling rates were under-predicted by around 18 pct, which was attributed to the neglect of heating due to plastic deformation of the stud material. The range of the peak temperatures and cooling rates suggests a martensitic phase formation for AISI 4140 steel.^[22] A higher hardness of the processed zone was thus expected compared to that in the unaffected substrate material.

Figures 9(a) through (c) show the estimated and the corresponding measured hardness results at a height of 8.0 mm from the base of the crack hole at three different force rates of 2, 4, and 8.0 kN/s, respectively. The hardness values remained high around 650 HV and uniform for the complete joint region up to the original crack-hole wall and depicted a sharp drop afterwards. The width of the region with higher hardness increased at greater stud force rates as higher forces resulting in a wider region with a high peak temperature as shown in Figure 6. The high hardness in the processed joint region was attributed to the formation of harder phases such as martensite due to the high hardenability of AISI 4140 and steep cooling rate. Figure 9(a) exhibits traces of localized high-hardness spikes in the stud-substrate clearance region, which is filled by the stud material at high strain rates and temperature during FHPP. As the FHPP joint is not tempered afterwards, such hardness variations in regions of high deformation and temperature gradient are perhaps expected.

Figures 10 and 11 show the computed and corresponding measured hardness values across the processed joint region at a typical height of 5.0 mm and along the base of the crack-hole base, respectively. The nature of variations of the hardness distribution across the joint regions in Figure 10 was nearly the same as that noted in Figure 9 except that the width of the high-hardness regions were slightly smaller in Figure 10. This was

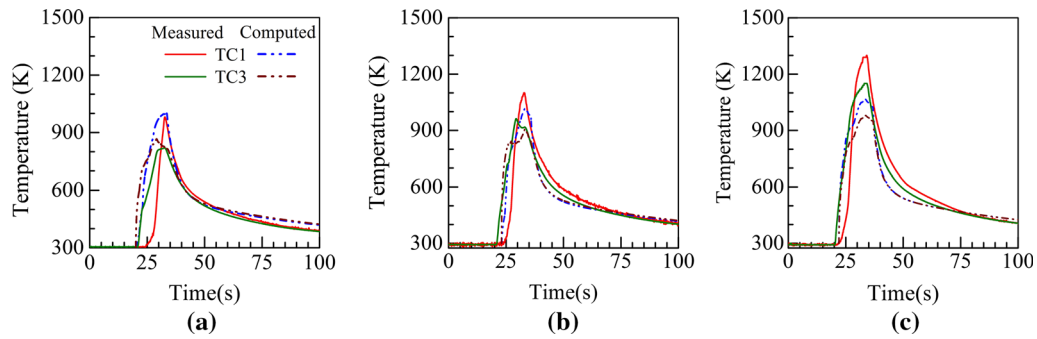


Fig. 8— Computed and corresponding measured thermal cycles at selected thermocouple locations TC1 and TC3 of during FHPP of AISI 4140 steel at stud force rate (kN/s) of (a) 2.0, (b) 4.0 and (c) 8.0 (Color figure online).

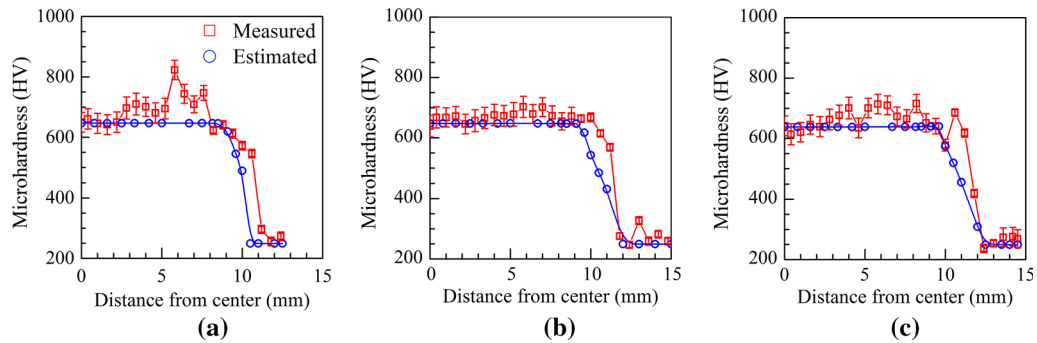


Fig. 9— Measured vis-à-vis estimated hardness at a height of 8.0 mm above the crack-hole base at stud force rates (kN/s) of (a) 2.0, (b) 4.0 and (c) 8.0.

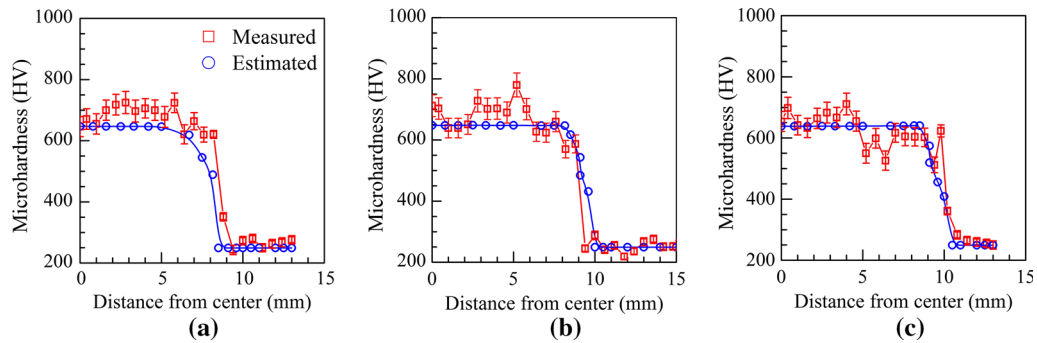


Fig. 10— Measured vis-à-vis estimated hardness at a height of 5.0 mm above the crack-hole base at stud force rates (kN/s) of (a) 2.0, (b) 4.0 and (c) 8.0.

attributed to the reduced peak temperature and cooling rate experienced at a lower height of 5.0 mm. Closer to the crack-hole base, both peak temperatures and cooling rates of the joint region reduced further; as a result, the width of the processed region with higher hardness values decreased further as depicted in Figure 11. The experimentally measured hardness values in Figure 11 were consistently higher than the corresponding computed results, attributed to the fine-grained structure of the material and presence of hard martensite phase. However, the effect of grain size was not considered in

empirical relations used for the estimation of hardness. A comparison of Figures 9, 10, and 11 show that the maximum width of the high-temperature region reduced from around 8.5 to 4.0 mm from the top to the bottom for the processing conditions considered here.

The measured average hardness values within the processed zone were in the range of 620 to 750 HV, and the corresponding computed values were 525 to 650 HV. The slight under-prediction in the computed hardness values was attributed to the simplified empirical relations that remained The numerically computed

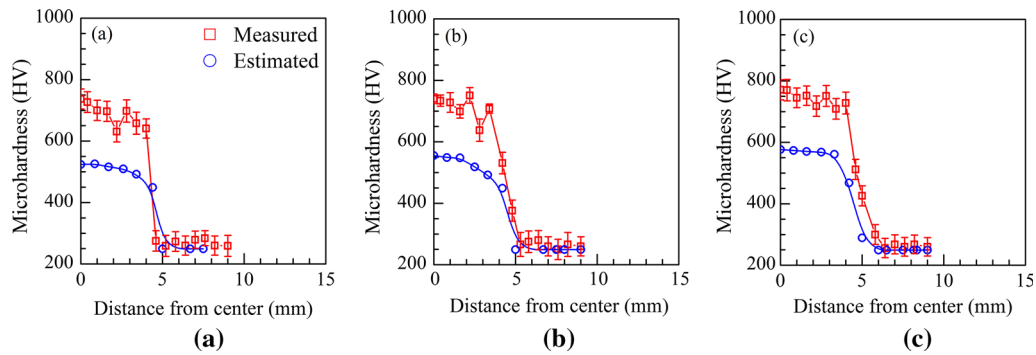


Fig. 11— Measured vis-à-vis estimated hardness along the base of the crack hole at stud force rates (kN/s) of (a) 2.0, (b) 4.0 and (c) 8.0.

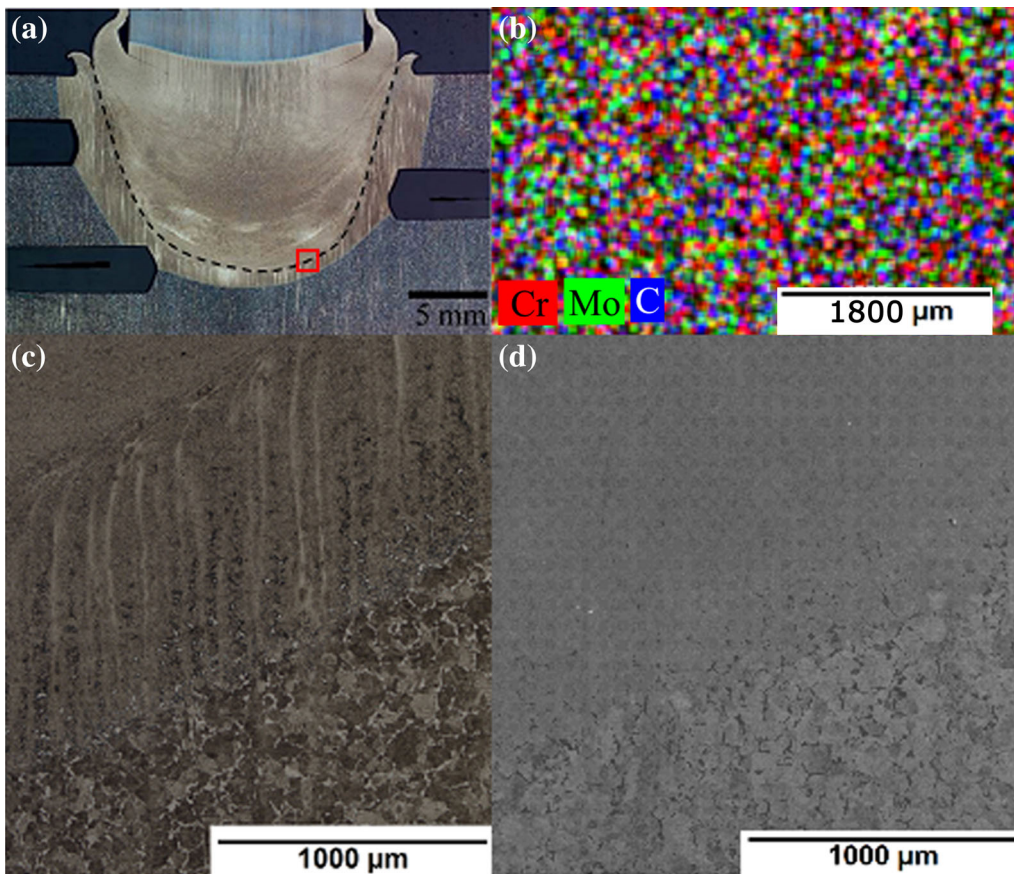


Fig. 12— (a) FHPP joint macrograph for the force rate of 2 kN/s and (b) EDS image, (c) optical micrograph and (d) SEM backscattered image of a selected region including stud-substrate joint and the adjacent regions as shown by the red open box in (a) (Color figure online).

temperature field and thermal cycles depict the ranges of peak temperature around 1200 to 1500 K and cooling rates around 45 to 130 K/s (between 1073 and 773 K) for the FHPP conditions considered here. Such cooling rate ranges are expected to result in a predominant martensitic structure in the processed zone of AISI 4140.^[23] Figure 12 shows the FHPP joint at a force rate of 2 kN/s and typical EDS analysis and images from optical microscopy (OM)

and scanning electron microscopy (SEM) of a localized region as shown by a red box in Figure 12(a). Detailed examination of the results from EDS, OM and SEM analyses did not reveal the presence of a tempered martensitic structure or carbide concentration. In addition, the EDS results showed a homogeneous distribution of Cr, Mo and C with no indication of regions with higher element concentration.

An attempt is made further to explain the likely formation of a martensitic structure by superimposing the cooling curves (Figure 7(c)) on a typical CCT (continuous-cooling-transformation) diagram of AISI 4140 in Figure A1 (Appendix A).^[24] Figure A1 confirms that the martensite phase transformation in the processed zone is expected and illustrates the application of the hardness estimation algorithm as presented in Appendix A. Hattingh *et al.*^[7] reported a similar range of hardness values in FHPP of AISI 4140 steel, and Corovilla *et al.*^[24] also reported similar values in laser hardening of AISI 4140 steel.

In summary, a coupled experimental and numerical analysis was carried out to study the effect of force rate and other key process variables in FHPP of AISI 4140 steel. An axisymmetric transient heat conduction model was developed to compute temperature field and thermal cycles. Adequate filling of the stud-crack-hole clearance and sound joint structure was obtained at a lower stud force rate of 2.0 kN/s, while the joints showed voids near the crack-hole bottom when FHPP was performed at higher force rates of 4.0 and 8.0 kN/s. Also, a lower force rate needed greater processing time to fill-up the crack hole, resulting in a smaller joint region with high hardness values. The computed thermal cycles and subsequently estimated hardness values showed fair agreement with the corresponding measured results. The influence of residual stresses was not addressed in the current analysis, but nonetheless should have an important effect on component usage, since thermal and mechanical stresses are abundant. Further studies are in progress to measure and predict the profile and magnitude of residual stresses through the weld with the objective of creating a useful tool to assess the appliance of FHPP in steels.

V. CONCLUSIONS

The present study aimed to eliminate the most commonly reported voids and crack-like defects near the crack-hole base in friction hydro-pillar processing of steels. Force rate was considered one of the main input process variables in FHPP for the first time in the literature. Higher force rates decrease the processing time during the dwell stage and increase the formation of crack-like defects in the bottom situ of the filled substrate hole because of inadequate thermal softening and localized discontinuities. A gentler increase in contact force with time during the dwell stage is then

envisaged as the proper solution. All tested conditions presented martensite formation in the processed zone, and a transient heat transfer model could be used to simulate the thermal profiles and estimate material hardness with reasonable accuracy. This thoroughly validated heat transfer model can be further used for an estimation of temperature distribution, joint structure and properties.

ACKNOWLEDGMENT

The work was jointly supported by the Department of Science and Technology (Ministry of Science and Technology), India, and National Council for Science and Technological Development (CNPq of the Ministry of Science, Technology and Innovation), Federal Republic of Brazil.

APPENDIX A

The hardness distribution across the joint is estimated using the numerically computed cooling rate and holding time between 1073 and 773 K at any given location and analytical-cum-empirical relations for prediction solid-state phase transformations and consequent hardness for steels of similar compositions available in the published literature.^[21] The cooling times to form either 50 pct martensite (Δt_M) or 50 pct bainite (Δt_B) are estimated as

$$\Delta t_M = 10^{(8.79C_{EQ}-1.52)}; \Delta t_B = 10^{(8.84C_{EQ}-0.74)} \quad [A1, A2]$$

where C_{EQ} is the carbon equivalent and considered as [International Institute of Welding].

The maximum volume fraction (V_{MAX}) undergoing solid-state phase transformations is estimated as a function of peak temperature (T_P) and percent of carbon content (C) in steel as

$$V_{MAX} = \begin{cases} 0 & \text{if } T_P \leq A_1 \\ \left(\frac{T_P-A_1}{A_3-A_1}\right) + \left(\frac{C}{0.83}\right) \left(\frac{A_3-T_P}{A_3-A_1}\right) & \text{if } A_1 < T_P \leq A_3 \\ 1 & \text{if } T_P > A_3 \end{cases} \quad [A3]$$

where A_1 and A_3 are respectively the lower and upper critical temperatures for austenite formation and typically correspond to 1013 and 1293 K, respectively, for

Table A1. Sample Hardness Calculation From Computed Temperature History

C	C_{EQ}	T_P (K)	CR (K s ⁻¹)	Δt (s)	Δt_M (s)	Δt_B (s)	V_{MAX}
0.39	0.77	1473.18	107.14	2.80	1.70e6	1.10e7	1.0
V_M	V_B	V_{FP}	H_M (HV)	H_B (HV)	H_{FP} (HV)	H (HV)	
1.0	0.0	0	647.33	430.07	250.52	647.33	

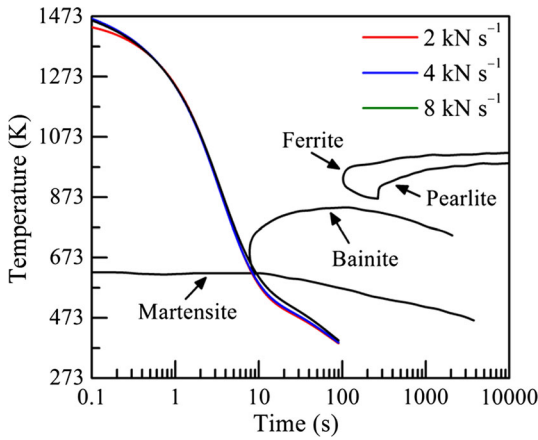


Fig. A1— Cooling curves [from Fig. 7(c)] superimposed on CCT (continuous-cooling-time) diagram of AISI 4140 steel.^[24] (Color figure online).

AISI 4140 steel. The volume fractions of martensite (V_M), bainite (V_B) and perlite-ferrite (V_{FP}) were estimated next as

$$V_M = V_{\max} \exp \left[-0.69(\Delta t / \Delta t_M)^2 \right] \quad [\text{A4}]$$

$$V_B = V_{\max} \exp \left[-0.69(\Delta t / \Delta t_B)^2 - V_M \right] \quad [\text{A5}]$$

$$V_{FP} = 1 - V_M - V_B \quad [\text{A6}]$$

where Δt was the total cooling time from 1073 to 773 K. The Vickers hardnesses of different constituent phases were computed as

$$H_M = 127 + 949C + 27Si + 11Mn + 8Ni + 16Cr + 21 \log(\text{CR}) \quad [\text{A7}]$$

$$H_B = -323 + 185C + 330Si + 153Mn + 65Ni + 144Cr + 191Mo + (89 + 53C - 55Si - 22Mn - 10Ni - 20Cr - 33Mo) \log(\text{CR}) \quad [\text{A8}]$$

$$H_{FP} = 43 + 223C + 53Si + 30Mn + 12.6Ni + 7Cr + 19Mo + (10 - 19Si + 4Ni + 8Cr + 130V) \log(\text{CR}) \quad [\text{A9}]$$

where (CR) is the computed cooling rate from 1073 K to 773 K. The net hardness (H) at any location is therefore estimated as

$$H = H_M V_M + H_B V_B + H_{FP} V_{FP} \quad [\text{A10}]$$

A sample calculation is shown in Table A1 for the estimation of hardness from the computed thermal history in FHPP of AISI 4140 steel. The calculations correspond to the thermal cycle shown in Figure 7(c) at a force rate of 4.0 kN/s. Figure A1 shows cooling curves from Figure 7(c) superimposed on a CCT diagram for AISI 4140 steel.^[24]

REFERENCES

1. D.L.H. Bulbring., D.G. Hattingh., A. Botes., and D.H. Odendaal: *J. S. Afr. Inst. Min. and Metall.*, 2013, vol. 113, pp. 129–36.
2. P.J. Hartley: *Weld. Met. Fab.*, 2000, vol. 9, pp. 6–8.
3. D.G. Hattingh, M.N. James, M. Newy, R. Scheepers, and P. Doubell: *Theor. Appl. Fract. Mech.*, 2016, vol. 83, pp. 125–34.
4. S. Liu, J.E. Indacochea: *Metals Handbook*, 10th ed., American society for Metals, Ohio, 1992.
5. V.H.C. de Albuquerque, C.C. Silva, C.R.O. Moura, W.M. Aguiar, and J.P. Farias: *Mater. Des.*, 2009, vol. 30, pp. 1068–74.
6. D.T. Buzzatti, J.T. Buzzatti, R.E. dos Santos, F. Mattei, M. Chludzinski, and T.R. Strohaecker: *Soldagem & Inspecao*, 2015, vol. 20, pp. 287–99.
7. D.G. Hattingh, D.L.H. Bulbring, A. Els-Botes, M.N. James: *Mater. Des.*, 2011, vol. 32, pp. 3421–30.
8. Y. Yin, X. Yang, L. Cui, F. Wang, and S. Li: *Mater. Des.*, 2015, vol. 88, pp. 990–98.
9. C.P. Meinhardt, M. Chludzinski, R.F. Ribeiro, C.L.F. Rocha, A.C.S. Santos, and T.R. Strokaecker: *J. Mater. Process. Technol.*, 2017, vol. 246(1), pp. 158–66.
10. *ASM Handbook, Properties and Selection: Irons, Steels, and High-Performance Alloys*, vol. 1, ASTM International, 2008, pp. 1–1063.
11. C.C. Silva, V.H.C. de Albuquerque, C.R.O. Moura, W.M. Aguiar, and J.P. Farias: *J. Mater. Process. Technol.* 2009, vol. 18, pp. 324–31.
12. M. Chludzinski, M.P. Paes, F.L. Bastian, and T.R. Strohaecker, *Mater. Des.*, 2012, vol. 33, pp. 340–44.
13. A. Meyer: Master's dissertation, Technical University Brunswick, Germany, 2002. https://www.hzg.de/imperia/md/content/hzg/zentrale_einrichtungen/bibliothek/berichte/gkss_berichte_2003/gkss_2003_4pdf, Accessed 03 October, 2017.
14. B. Vicharapu, L.F. Kanan, T. Clarke, and A. De: *Sci. Technol. Weld. Join.*, 2017, vol. 22, pp. 555–61.
15. S.J. Unfried, M.T.P. Paes, T.F.C. Hermenegildo, F.L. Bastian, and A.J. Ramirez: *Sci. Technol. Weld. Join.*, 2015, vol. 15, pp. 506–13.
16. C.R.L. Lessa, D. Martina, A.P. Figueireira, B.F. Machado, F. Claudiam, and T.R. Strohaecker: *Materials Research*, 2015, vol. 19, pp. 928–36.
17. L. Cui, X. Yang, D. Wang, X. Hou, J. Cao, and W. Xu: *Mater. Sci. Eng. A*, 2014, vol. 611, pp. 15–28.
18. ASTM E230/E230M, ASTM International, 2011, Pennsylvania, USA.
19. R. Nandan, G.G. Roy, T.J. Lienert, and T. Debroy: *Acta. Mater.*, 2007, vol. 55, pp. 883–95.
20. V. Buchibabu, G.M. Reddy, and A. De: *J. Mater. Process. Technol.*, 2017, vol. 241, pp. 86–92.
21. J.C. Ion, K.E. Easterling, and M.F. Ashby, *Acta. Metall.*, 1984, vol. 32, pp. 1949–62.
22. R.S. Lakhkar, Y.C. Shin, and M.J.M., Krane: *Mat. Sci. Eng. A*, 2008, vol. 408, pp. 209–17.
23. *ASM Handbook, Steel Heat Treating Fundamentals and Processes*, vol. 4, ASTM International, 2013, pp. 1–784.
24. F. Cordovilla, A. Garcia-Beltran, P. Sanho, J. Domingues, L. Ruiz-de-Lara, J.L. Ocana: *Mater. Des.*, 2016, vol. 102, pp. 225–37.